Pressure dependent wall slip of wood flour filled polymer melts

Article *in* Journal of Non-Newtonian Fluid Mechanics · July 2017

DOI: 10.1016/j.jnnfm.2017.07.002

2 authors:

Valentina Mazzanti
University of Ferrara

Francesco Mollica
University of Ferrara

Pressure dependent wall slip of wood flour filled polymer melts

Valentina Mazzanti and Francesco Mollica

Dipartimento di Ingegneria, Università degli Studi di Ferrara, Via Saragat 1, I - 44122 Ferrara, Italia

Corresponding author: F. Mollica, francesco.mollica@unife.it, +39 329 750 6547

Abstract

The rheological properties of a 50 wt.% wood flour filled polypropylene have been measured at 195°C using an instrumented slit die attached to a single screw extruder. Wall slip and non-Newtonian effects have been corrected through the Mooney and Rabinowitsch procedures, thus equations for viscosity and wall slip have been obtained. Interestingly, the pressure drop profiles calculated using these equations are not perfectly consistent with the experimental pressure measurements, in that the theoretical curves overestimate the experimental data. An explanation has been sought by assuming that slip velocity increases in the last portion of the slit die, i.e. close to the exit, where pressure drops down considerably. A pressure dependent slip model has been then proposed, its specific equations numerically solved and the results fitted to the experimental pressure data. The fitting is better than the one coming from the model that comprises slip depending on shear stress only, thus, for the fluid that has been studied, the assumption of pressure dependent slip appears to be justified.

Keywords: Wood polymer composite, wall slip, in-line rheometry, modeling, pressure dependence

1. Introduction

Natural fiber filled polymers combine environmental friendliness with typical advantages of plastics materials (e.g. formability, lightness, etc.) and this is the reason for the relatively large body of dedicated research available in the present-day scientific literature (Gurunathan et al. 2015; Pickering et al. 2016). Although some natural fibers can increase the mechanical properties, much in the same way as more traditional reinforcements such as glass fibers, still their main appeal is cost reduction. From this point of view, filling with high concentrations of natural fibers is most convenient. On the other hand, this can increase compound viscosity remarkably, thus processing becomes a challenging task and natural fiber degradation due to excessive localized viscous heating is a constantly present pitfall.

Processing can become easier thanks to wall slip, which is a characteristic of polymeric suspensions such as this one (Li and Wolcott 2005). More precisely, in the case of suspensions, it

is well known (Vinogradov and Ivanova 1967; Barnes 1995; Kalyon 2005; Pieper 2015) that flow induced hydrodynamic forces push suspended particles away from solid walls, thus creating a solute depleted and less viscous layer in close contact with the boundary. This has the effect of lubricating the suspension flow at the wall, leading to what is termed apparent slip. However, whether apparent or real, suspensions slip can be studied and characterized with the same means as usual wall slip. Moreover, external lubricants are often added to highly filled compounds in order to ease passage through processing machineries even further and contribute to apparent wall slip.

In spite of being an advantage for processing, slip may lead to measurement errors when it occurs in a viscometer and is not taken into account properly. In the case of pressure driven flow viscometry, the Mooney procedure (Mooney 1931) was developed as a correction of the well-known Rabinowitsch procedure. For capillary viscometry, it consists in running measurements through capillaries of different radii and estimating the slip corrected apparent shear rate by extrapolating curves of apparent shear rate as a function of the inverse radius, plotted at constant wall shear stress, down to inverse radius tending to zero.

The Mooney procedure does not work always: it is necessary that the constant shear stress curves be straight lines and that their intercept with the apparent shear rate axis be positive. Most notable cases where the Mooney procedure fails are in the case of concentrated suspensions of ceramic powders and polymeric fluids of elastomeric nature (Jastrzebski 1967; Mourniac et al. 1992). Here the Mooney lines are often curved upwards and have negative extrapolated intercepts with the apparent shear rate axis.

The reasons for the failure of the Mooney procedure might be related to some of its underlying assumptions. In particular, the flow is assumed to be fully developed, i.e. the velocity components must be independent of the axial coordinate, which in turn implies that pressure needs to vary linearly with axial distance and that the wall shear stress has to be constant throughout the whole channel length. As a consequence, the slip velocity must also be uniform along the channel, thus it may depend on the shear component of local stress but not on pressure (or more precisely wall normal stress): as pressure varies with the axial coordinate, it would induce non-full development.

Pressure dependent wall slip has been widely investigated in a number of papers. Early evidences that slip increases with decreasing pressure date back to Vinogradov and Ivanova (1967). A simple but effective pressure dependent slip model has been introduced by Hill et al. (1990) and used in a number of papers (e.g. Person and Denn 1997 among others). A systematic experimental study at the capillary rheometer of pressure dependent slip of polyolefins, together with a very thorough mathematical model, is due to Hatzikiriakos and Dealy (1992), while a theoretical study of pressure dependent wall slip of Newtonian fluids without neglecting inertia is due to Rao and Rajagopal (1999). Tang and Kalyon (2008) and Tang (2012) have solved some pressure dependent slip flows of non-Newtonian compressible suspensions and compared them with experimental results obtained using polydimethylsiloxane as a test fluid. More recently, Kalogirou et al. (2011),

Damianou et al. (2013) and Housiadas (2013) have solved theoretically and numerically some flows of incompressible Newtonian and non-Newtonian fluids with pressure dependent slip.

In this paper we will consider a natural fiber filled polymer melt. Its rheological properties will be evaluated using an in-line slit viscometer. Pressure will be measured at three specific locations along the instrumented slit die and the pressure gradient will be derived accordingly. It will be shown that the pressure drop diagram is non-linear and the resulting non-fully developed flow can be explained on the basis of pressure dependent wall slip. A pressure dependent wall slip constitutive law will then be introduced and its results compared with the experimental measurements.

2. Experimental materials and methods

The fluid considered in this investigation is a molten wood polymer composite (WPC). Specifically, it is a polypropylene melt filled with 50 wt.% white fir wood flour. It has been purchased from PlasticWOOD S.r.l., Mazzantica di Oppeano (VR), Italy, as a commercial compound (PP 50 SCD), its mechanical and thermal characterization can be found in (Mazzanti and Mollica 2016).

A slit die in-line rheometer attached to a single screw extruder (P.R.T. SERVICE & INNOVATION s.r.l., Sant'Agostino (FE), Italy) has been used to perform the rheological measurements. This instrument is described in (Mazzanti and Mollica 2015), where also measurement uncertainties are evaluated and reported. The main characteristics of the in-line rheometer will be outlined here briefly.

The slit die has a length of 105 mm and a width of 50 mm, it is made of AISI 4317 steel, case hardened and tempered to HRC 61. Three flush mounted pressure transducers (GEFRAN M32 type mercury–filled transducers, ± 0.25% full scale accuracy) allow pressure drop measurements along the die. The first pressure transducer (200 bar full scale) is placed 40 mm after the slit entrance in order to reduce the influence of entrance effects. The remaining two transducers are located 25 mm apart, hence at 65 mm and 90 mm from the entrance (100 bar and 50 bar full scale, respectively), thus making the overall measurement length equal to 50 mm. The pressure measurements are used to calculate the pressure gradient along the die.

Slit die temperature is controlled through three thermostat operated resistance heaters. A more direct measure of the fluid temperature is also realized thanks to thermocouples (J-type, ± 0.1 °C accuracy) embedded within the pressure transducers. The slit gap is adjustable (see Kalyon and Gokturk 1994 and Kalyon et al. 2006a) and this allows to perform the Mooney correction procedure. In this study, slit gaps of 1.95, 2.45, 3.31, 4.04 mm have been used.

The WPC pellets have been dried at 80°C for 24 hours before being flood fed into the extruder to perform the rheological measurements. A uniform temperature distribution of 195°C has been set along the extruder barrel and the slit die.

The mass flow rate has been measured by dividing the throughput weight (weighed with a precision scale) by the time needed to extrude it. The volumetric flow rate has been determined by dividing the mass flow rate by the known density of the fluid at the testing temperature (1025 kg/m^3).

3. Experimental results

The average temperature readings at the three transducer locations are pictured in Fig. 1 for the four slit dies. Even if a flat temperature profile of 195°C has been superimposed, only the temperature at the first transducer is almost equal to the set temperature, while the one at the middle transducer is slightly higher and the last one is lower. Most probably, the low temperature reading at the end is due to the proximity of the exit, while the heating in the middle of the die is compatible with flow induced viscous dissipation. Notice, in fact, that non-uniformity increases with decreasing the slit die gap. Difficulties in keeping a uniform temperature profile are a well-known problem of the present approach (Padmanabhan and Bhattacharya 1994). However, temperature discrepancies are within 2.5 °C from the target temperature, thus the experimental measurements that follow can be considered reliable.

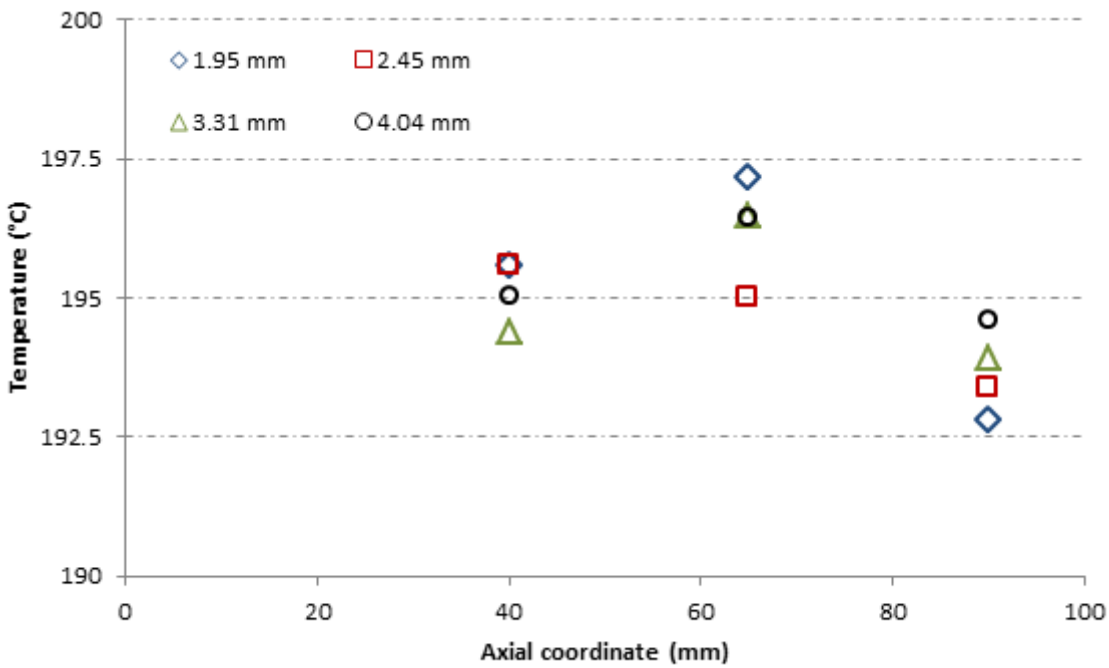

Fig. 1: Average temperature profiles for the flow in the various slit dies. Highest non-uniformity is for the thinnest slit

Concerning viscosity evaluation, let $\mathrm{grad}\, p$ indicate the pressure gradient, Q the volumetric flow rate and let W and H be the slit width and gap, respectively. The absolute value of the wall shear stress τ_w can be defined as:

$$\tau_w = -\frac{H}{2}\,\mathrm{grad}\, p\ , \qquad (1)$$

while the apparent wall shear rate $\dot{\gamma}_{app}$, i.e. the shear rate the fluid would have if it were Newtonian, is:

$$\dot{\gamma}_{app} = \frac{6Q}{WH^2} \,. \tag{2}$$

The shear stress vs. apparent shear rate curves for the four different slit gaps are shown in Fig. 2. The four curves do not coincide: going from left to right they are placed from the thickest to the thinnest die. This is a clear indication of wall slip, thus the Mooney procedure can be attempted to correct for slip.

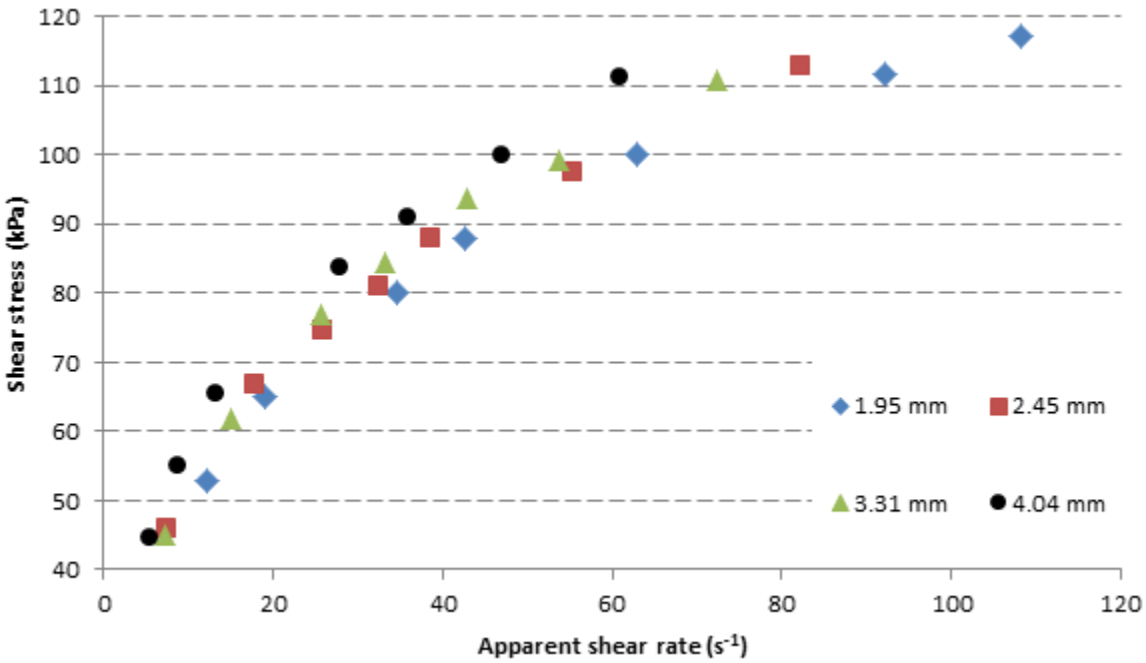

Fig. 2: Wall shear stress vs. apparent shear rate for the four slit gaps. Besides being non coincident, the curves place themselves left to right from thickest to thinnest

The resulting Mooney plot is displayed in Fig. 3. As can be seen, the constant shear stress data points are not perfectly aligned along straight lines, but forcing a linear fit one obtains a positive intercept with the ordinate axis. In a case like this one it is customary to assume the Mooney procedure to be valid. The slip velocity U_s and the apparent shear rate clear of the contribution of wall slip, here indicated with $\dot{\gamma}_{app\ no\ slip}$, can be obtained using the following equation:

$$\dot{\gamma}_{app} = \frac{6\,U_s}{H} + \dot{\gamma}_{app\ no\ slip} \,. \tag{3}$$

This apparent shear rate has to be further processed with the Rabinowitsch correction to take into account non-Newtonian effects, so that the true shear rate $\dot{\gamma}$ can be finally obtained. The shear viscosity η is then given by the usual definition:

$$\eta = \frac{\tau_w}{\dot{\gamma}} \,. \tag{4}$$

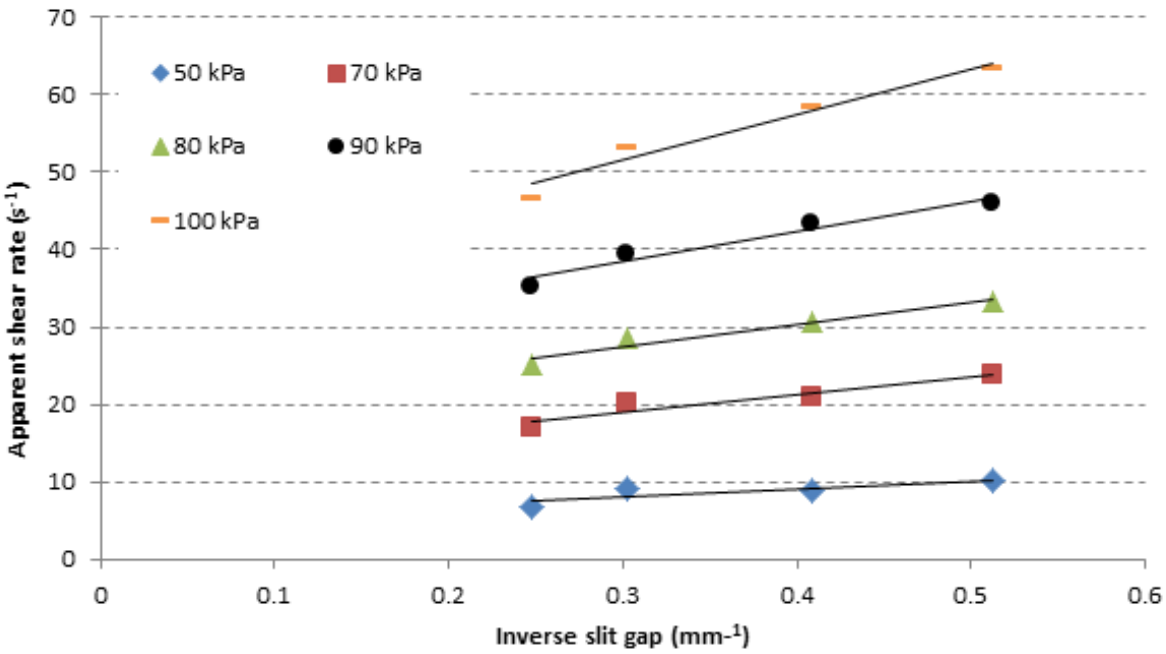

Fig. 3: Mooney plot for five values of constant wall shear stress. Linear fit is approximate but the intercept with the shear rate axis is positive for all values of shear stress.

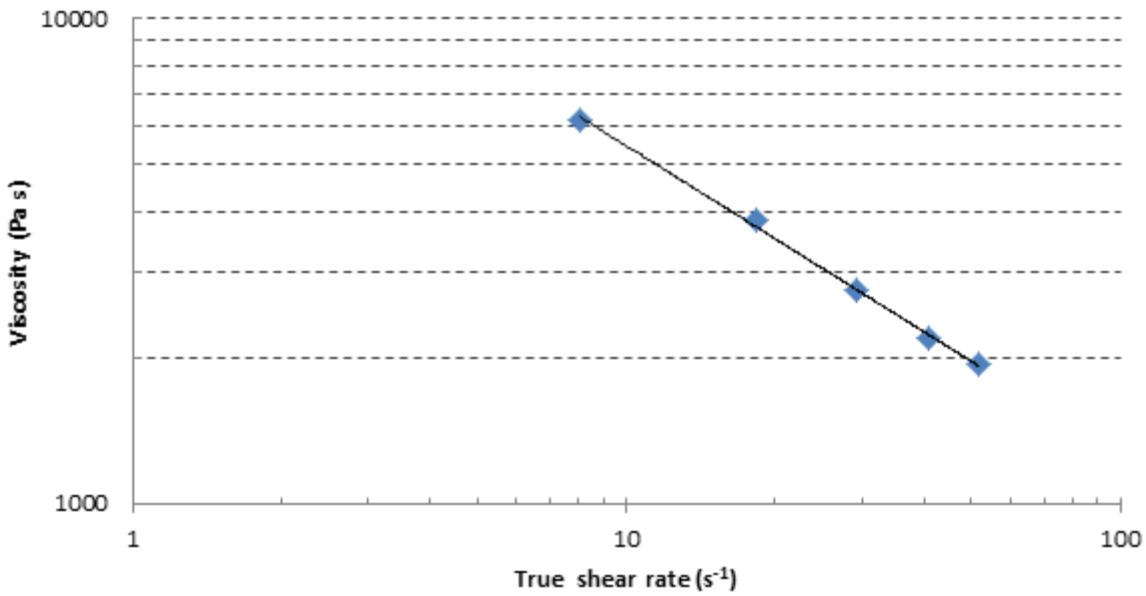

Fig. 4: Viscosity vs. true shear rate. The points align in a log-log plot, thus a good fitting is provided by the power law of Eq. (5)

In Fig. 4 the plot of viscosity as a function of true shear rate is pictured together with its power law model fitting:

$$\eta = \bar{k}\,\dot{\gamma}^{\bar{n}-1}\ . \qquad (5)$$

The slip velocity as a function of wall shear stress is shown in Fig. 5 and it also can be fitted with a power law:

$$U_s = \bar{\chi}\, \tau_w{}^{\bar{m}} \,. \tag{6}$$

The parameters used to fit Eqs. (5) and (6) are reported in Tab. 1. Fitting of both curves is quite satisfactory, especially concerning viscosity.

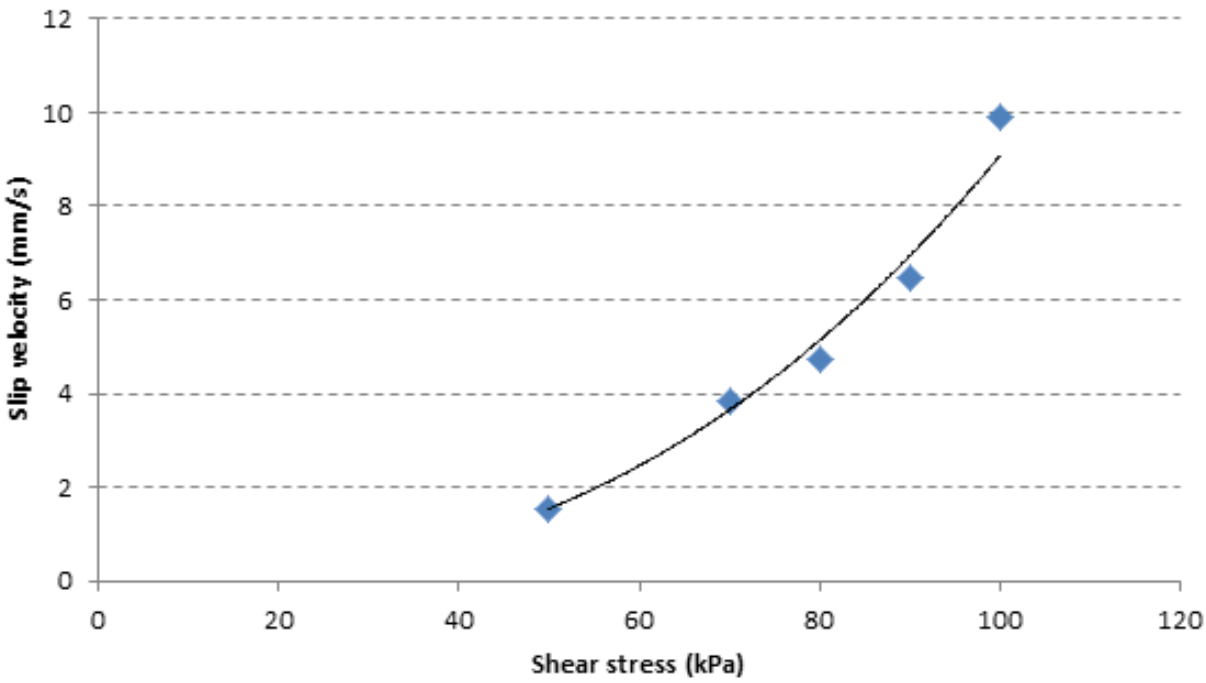

Fig. 5: Slip velocity as a function of wall shear stress and curve fitting using Eq. (6). Fitting is reasonable but not completely satisfactory

Tab. 1: Material parameters for viscosity and slip law resulting from the Mooney-Rabinowitsch procedure

Viscosity power law Eq. (5)		Slip law Eq. (6)	
$\bar{k}$ $(kPa\, s^{-\bar{n}})$	$\bar{n}$	$\bar{\chi}$ $(m/s\ Pa^{-\bar{m}})$	$\bar{m}$
23.7	0.364	1.61 10^{-15}	2.55

Now, the model that has been obtained (Eqs. 5 and 6 with the parameter values of Tab. 1) can be used to reproduce the experimental plots of pressure as a function of axial location: it can be done by solving for Poiseuille flow in the slit imposing the same experimentally measured flow rate Q, or the average fluid velocity:

$$U = \frac{Q}{WH} \,. \tag{7}$$

These plots can be compared to the experimental pressure measurements directly. A few examples are shown in Fig. 6: the model curves are indeed rather close to the experimental data but all of them overestimate the pressure measurements by a certain amount.

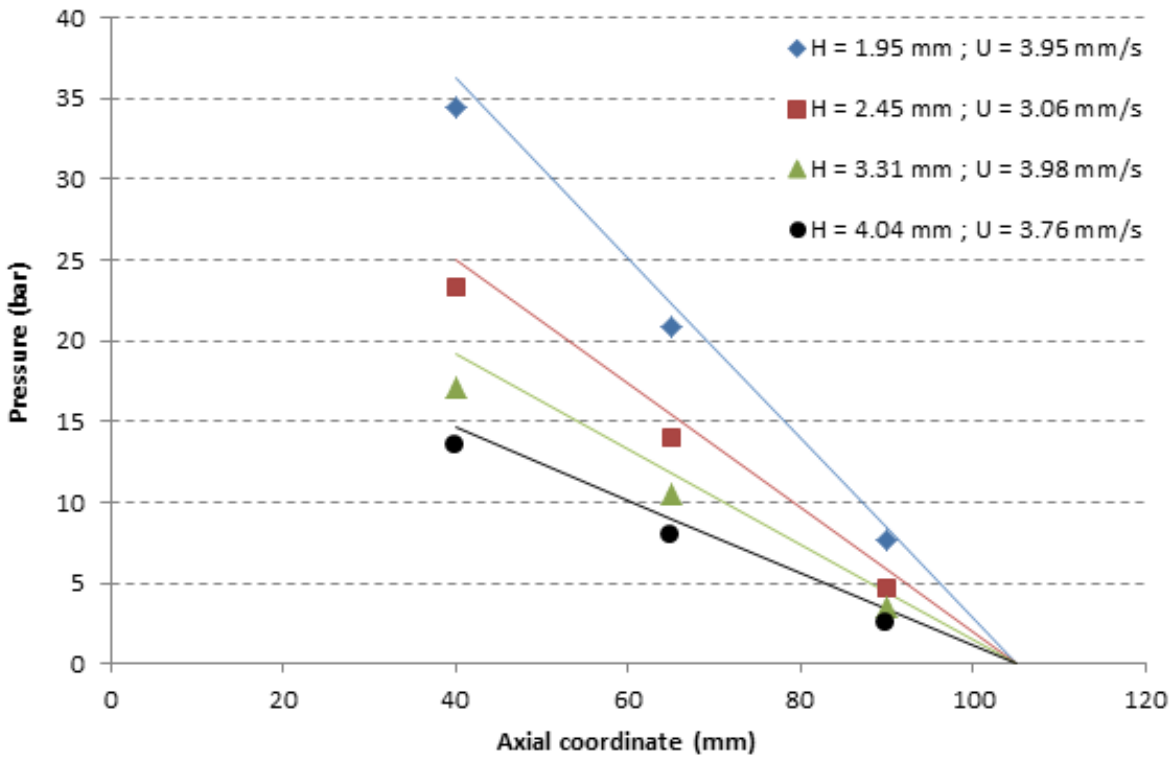

Fig. 6: Experimental pressure measurements (dots) and model predictions (continuous lines) coming from Eqs.(5) and (6) with the parameter values of Tab. 1 (i.e. using the Mooney-Rabinowitsch procedure). Overestimation is quite evident

In order to show this feature better, we have reported in Tab. 2 all of the experimental pressure values measured at the three transducer locations (in white background), together with the theoretical values estimated at the same locations on the basis of the model coming from the Mooney-Rabinowitsch procedure (in yellow background). In order to quantify the comparison, the values of the absolute and normalized errors are also reported in Tab. 2. They are defined as:

$$\text{Absolute error} = p_{md} - p_{xp} \qquad \text{Normalized error} = \frac{p_{md} - p_{xp}}{p_{xp}} * 100, \tag{8}$$

where the quantity p_{xp} stands for an experimental pressure measurement at the first, second or third axial location, while p_{md} is the corresponding model estimate. Red background color is used to highlight model points that overestimate experimental values, while blue background color means underestimation. It can be seen that all but three values are overestimated. The model overestimating the experimental values is a qualitative error: from the quantitative point of view, in fact, the equations coming from the Mooney-Rabinowitsch procedure behaves fairly well, but the presence of a qualitative error indicates that something in the physics of the problem is not adequately captured. This is especially true at low pressure values.

Tab. 2: Experimental pressure values compared with pressure values obtained with the model coming from the Mooney-Rabinowitsch procedure

		Experimental data			Mooney-Rabinowitsch			Absolute error			Normalized error		
H (mm)	U (mm/s)	p1 (bar)	p2 (bar)	p3 (bar)	p1 (bar)	p2 (bar)	p3 (bar)	p1 (bar)	p2 (bar)	p3 (bar)	p1 (%)	p2 (%)	p3 (%)
1.95	3.95	34.46	20.88	7.70	36.30	22.34	8.38	1.84	1.46	0.67	5.32	6.97	8.74
	6.20	42.32	25.44	9.01	43.01	26.47	9.93	0.68	1.02	0.92	1.62	4.02	10.20
	11.22	52.60	31.88	11.59	53.79	33.10	12.41	1.18	1.22	0.83	2.25	3.81	7.13
	13.83	57.48	34.56	12.42	58.18	35.81	13.43	0.71	1.24	1.01	1.23	3.59	8.15
	20.45	65.64	39.58	14.33	67.41	41.48	15.56	1.77	1.91	1.22	2.70	4.82	8.52
	29.97	73.64	44.50	16.32	77.82	47.89	17.96	4.18	3.39	1.63	5.68	7.63	10.01
	35.14	77.24	46.74	17.19	82.62	50.84	19.07	5.37	4.10	1.88	6.96	8.78	10.92
2.45	3.06	23.35	14.06	4.62	25.06	15.42	5.78	1.71	1.36	1.17	7.32	9.68	25.31
	7.26	34.67	21.07	7.38	34.65	21.32	8.00	-0.02	0.25	0.62	-0.05	1.21	8.41
	10.54	39.20	24.03	8.72	39.86	24.53	9.20	0.66	0.50	0.48	1.67	2.07	5.53
	13.30	42.19	25.64	9.12	43.49	26.76	10.04	1.30	1.12	0.92	3.09	4.38	10.07
	15.80	45.94	27.94	10.02	46.39	28.55	10.70	0.45	0.61	0.68	0.98	2.17	6.79
	22.57	51.30	31.38	11.54	53.01	32.62	12.23	1.71	1.24	0.69	3.33	3.96	5.97
	33.63	59.34	36.19	13.32	61.55	37.87	14.20	2.20	1.68	0.88	3.71	4.65	6.62
3.31	3.98	17.10	10.45	3.52	19.14	11.78	4.42	2.03	1.32	0.90	11.88	12.64	25.47
	8.34	23.83	14.61	5.15	25.21	15.52	5.82	1.38	0.91	0.67	5.80	6.22	12.97
	14.16	29.86	18.29	6.62	30.71	18.90	7.09	0.85	0.61	0.46	2.85	3.31	7.00
	18.30	33.00	20.31	7.49	33.80	20.80	7.80	0.79	0.49	0.31	2.41	2.40	4.17
	23.66	36.70	22.56	8.38	37.19	22.89	8.58	0.49	0.32	0.20	1.35	1.43	2.45
	29.65	38.39	23.46	8.40	40.45	24.89	9.34	2.06	1.43	0.94	5.36	6.10	11.18
	39.86	43.40	26.71	9.90	45.17	27.79	10.42	1.76	1.08	0.52	4.06	4.06	5.30
4.04	3.76	13.49	7.93	2.50	14.61	8.99	3.37	1.12	1.06	0.87	8.27	13.38	35.03
	6.06	17.06	10.16	3.46	17.45	10.74	4.03	0.39	0.57	0.57	2.28	5.66	16.35
	9.04	20.60	12.39	4.43	20.26	12.47	4.67	-0.35	0.08	0.25	-1.69	0.61	5.57
	18.85	26.56	16.07	5.91	26.62	16.38	6.14	0.05	0.31	0.24	0.19	1.91	3.98
	24.31	28.89	17.48	6.42	29.25	18.00	6.75	0.36	0.52	0.33	1.26	2.95	5.21
	31.76	31.82	19.31	7.12	32.30	19.88	7.45	0.48	0.57	0.34	1.51	2.95	4.73
	41.09	35.67	21.70	8.14	35.55	21.88	8.20	-0.12	0.17	0.06	-0.34	0.79	0.79

A possible reason for this behavior can be understood by looking at Fig. 7, which illustrates one representative experimental pressure profile together with its fitting based on the Mooney-Rabinowitsch procedure. The experimental points are aligned along a straight line, which would not cross the zero pressure axis at the channel exit (i.e. at 105 mm) but slightly behind. The pressure profile obtained from the model is parallel to the experimental one, meaning that the shear stress is in fact the same for both. On the other hand, the model pressure profile must meet zero pressure exactly at the die exit, since this is the pressure boundary condition. From an experimental point of view, pressure can indeed be different from zero at the die exit. In fact, this is a method for

estimating normal stress differences in pressure driven flows (Han 1974; Walters 1975). On the other hand, notice that in the present case the extrapolated pressure value would be negative, which is possible but unlikely. In any case, it is well known that the effects of the normal stress differences are relatively minor for suspensions (Aral and Kalyon 1997), thus it is plausible that pressure is indeed very close to zero at the die exit.

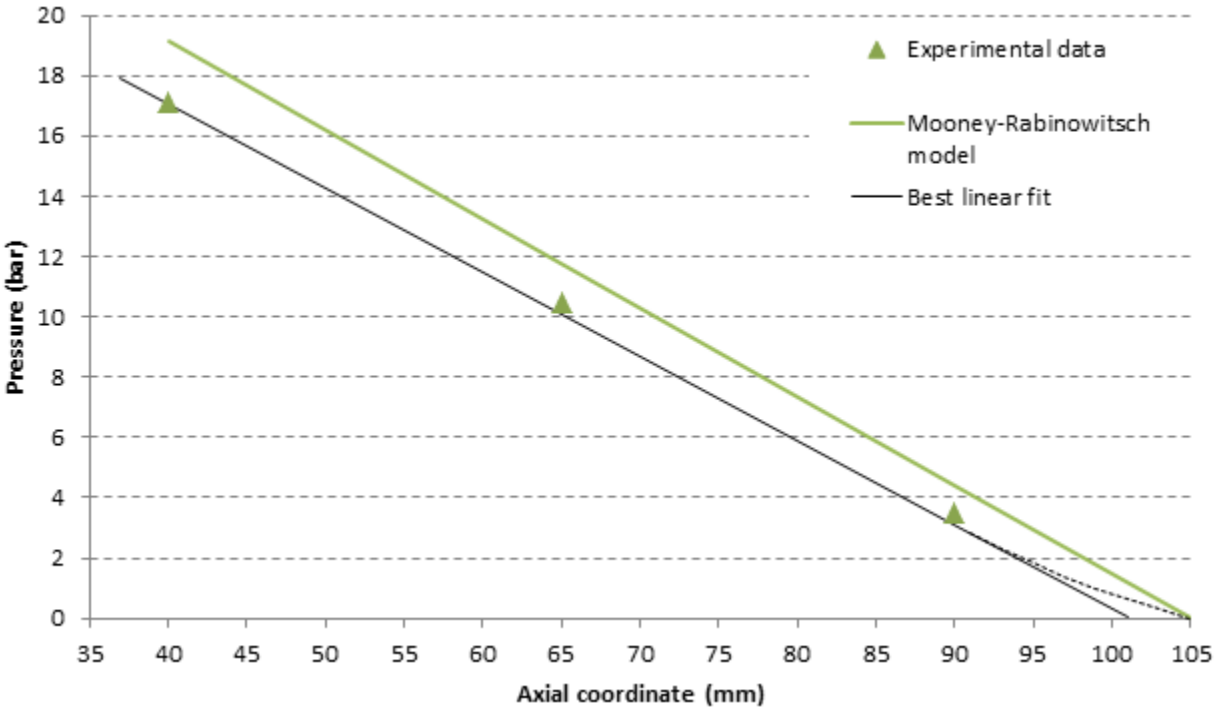

Fig. 7: Despite alignment of the experimental points, the extrapolated intercept with the zero pressure axis falls short of the channel exit. This is an indication of non-linearity of the pressure vs. axial location plot, which in turn points out to non-fully developed flow in the exit region. On the other hand, the pressure profile coming from the model constructed through the Mooney-Rabinowitsch procedure is linear and meets the zero pressure axis exactly at the channel exit.

If we assume that pressure is indeed zero at the exit, then the experimental pressure drop must lose linearity in the vicinity of the exit (see the dotted line of Fig. 7), bringing about a slight upward curvature of the pressure profile. Hence, in this region the flow will not be fully developed. The easiest explanation for this behavior is to assume a wall slip velocity increase in the vicinity of the die exit due to the local pressure decrease, in agreement with Vinogradov and Ivanova (1967). Slip, in fact, is definitely occurring, as it has been implied by the differences in the curves of Fig. 2. If slip velocity increases while keeping the flow rate constant, the effect on the flow is a decrease in the absolute value of the velocity gradient at the wall, i.e. the wall shear rate. This in turn determines a decrease in the wall shear stress and thus a less steep pressure profile slope.

Notice that non-full development could also be due to pressure dependent viscosity. In this case, though, non-linearity of the pressure profile should be seen along the whole channel length (see for instance the results of Kalogirou et al. 2011), not only at the channel end, whereas the

experimental pressure measurements of this study lie almost perfectly on a straight line everywhere but in the exit region.

4. Modeling

As discussed previously, a better fit of the experimental data would be obtainable if wall slip depended on wall normal stress in addition to shear stress. In this section a model of wall normal stress dependent slip will be introduced and solved for the flow in a rectangular slit. As the slit gap H is much smaller than both the slit length L and width W, the lubrication approximation can be used. It is convenient to identify L with the length between the first transducer and the die exit, thus we will consider $L = 65\ \mathrm{mm}$.

The flow domain is a rectangular area: the axial slit coordinate will be $0 \leq x \leq L$, while in the transverse direction the flow is assumed symmetric, thus the transverse coordinate will be $0 \leq y \leq H/2$. Moreover, the flow field is assumed two dimensional, with velocity components $u = u(x, y)$ along the axial direction of the die and $v = v(x, y)$ in the transverse direction. No flow is assumed in the direction of the slit width, i.e. secondary flows will be neglected. This hypothesis normally holds provided that the slit width is much greater than the gap. The fluid is also assumed to be incompressible.

According to the lubrication approximation, only the momentum equation in the axial direction needs to be considered:

$$\frac{\mathrm{d}p}{\mathrm{d}x} = \frac{\partial \tau_{xy}}{\partial y}. \tag{9}$$

Here $p = p(x)$ is the hydrostatic pressure and the notation τ_{xy} for the shear stress in the fluid is used also to highlight the dependency of shear stress on both x and y. Eq. (9) can be integrated once in y using the symmetry condition, i.e. $\tau_{xy}\big|_{y=0} = 0$, the result is

$$\tau_{xy} = \frac{\mathrm{d}p}{\mathrm{d}x} y = -\tau_w \frac{2y}{H} \tag{10}$$

where

$$\tau_w = \tau_w(x) = -\frac{\mathrm{d}p}{\mathrm{d}x}\frac{H}{2} \tag{11}$$

is the absolute value of the wall shear stress. In order to find the axial velocity, the material constitutive equation has to be specified. Fluids containing high amounts of filler usually exhibit an yield stress due to significant particle – particle interactions, while the molten polymeric matrix shows shear thinning effects. If these two phenomena occur together, a suitable mathematical model is the Herschel-Bulkley model: it is a generalized Newtonian fluid capable of modeling both shear thinning and yield. It does neglect viscoelasticity, but usually this is not considered to be an important limitation in the case of tube flow. The flow rule can be written as:

$$\dot{\gamma} = \frac{\partial u}{\partial y} = \begin{cases} 0 & |\tau_{xy}| \leq \tau_0 \\ \mathrm{sgn}(\tau_{xy}) \left(\frac{|\tau_{xy}| - \tau_0}{k}\right)^{\frac{1}{n}} & |\tau_{xy}| > \tau_0 \end{cases} \tag{12}$$

where τ_0 is the yield stress of the fluid and sgn(x) stands for the signum function, i.e. the function that extracts the sign of its argument. Now, in order to obtain the axial velocity, Eq. (12) is integrated once in y using the second of Eqs. (10) and the boundary condition

$$u|_{y=H/2} = U_s(x) \tag{13}$$

with $U_s(x)$ being the wall slip velocity. The result is:

$$u(x,y) = \begin{cases} U_s & \tau_w \leq \tau_0 \\ U_s + \frac{n}{1+n}\left(\frac{\tau_w}{k}\right)^{\frac{1}{n}}\frac{H}{2}\left(1-\frac{\tau_0}{\tau_w}\right)^{1+\frac{1}{n}} & \tau_w > \tau_0\,;\ \ 0 \leq y \leq \frac{\tau_0}{\tau_w}\frac{H}{2} \\ U_s + \frac{n}{1+n}\left(\frac{\tau_w}{k}\right)^{\frac{1}{n}}\frac{H}{2}\left[\left(1-\frac{\tau_0}{\tau_w}\right)^{1+\frac{1}{n}} - \left(\frac{2y}{H}-\frac{\tau_0}{\tau_w}\right)^{1+\frac{1}{n}}\right] & \tau_w > \tau_0\,;\ \ y > \frac{\tau_0}{\tau_w}\frac{H}{2} \end{cases} \tag{14}$$

This can be integrated once more in y between 0 and $H/2$ to yield the volumetric flow rate:

$$Q = 2W\int_0^{H/2} u(x,y)\mathrm{d}y\ , \tag{15}$$

which, by conservation of mass and incompressibility, has to be constant. Thus, indicating with U the average velocity, we have:

$$U = \frac{Q}{WH} = \begin{cases} U_s & \tau_w \leq \tau_0 \\ U_s + \frac{n}{1+n}\frac{H}{2}\left(\frac{\tau_w}{k}\right)^{\frac{1}{n}}\left(1-\frac{\tau_0}{\tau_w}\right)^{1+\frac{1}{n}}\left[1-\frac{n}{1+2n}\left(1-\frac{\tau_0}{\tau_w}\right)\right] & \tau_w > \tau_0 \end{cases} \tag{16}$$

This result is also present in Tab II of Kalyon (2005). The other constitutive equation that must be specified is the one for the slip velocity. This should be of the form $U_s = U_s(\tau_w, \sigma_w)$, with σ_w indicating the wall normal stress:

$$\sigma_w = p + \frac{N_1 - N_2}{3}\ . \tag{17}$$

In this equation, $N_1 = N_1(\dot{\gamma})$ and $N_2 = N_2(\dot{\gamma})$ indicate the first and second normal stress differences. There are experimental difficulties in measuring the normal stress differences (Aral and Kalyon 1997), especially at relatively high values of shear rate (Hatzikiriakos and Dealy 1992). On the other hand, there is experimental evidence (Hristov and Vlachopoulos 2007) that the quantity $N_1 - N_2$ measured through rotational rheometry is of the order 10^4 Pa (i.e. 0.1 bar) for a 20% wood flour filled high density polyethylene, and is a decreasing function of wood flour percentage. Moreover, during extrusion we noticed very little die swell, indicating low elastic properties of the suspension. Thus, for simplicity and as a first approximation, we propose to approximate the wall normal stress with pressure, i.e.

$$\sigma_w \approx p. \tag{18}$$

The specific form for the slip velocity equation that we propose is:

$$U_s = \begin{cases} \chi\,\tau_w^m & \tau_w \leq fp \\ \chi\,\tau_w^m + \lambda\,(\tau_w - fp)^m & \tau_w > fp \end{cases}. \tag{19}$$

This indicates that for relatively high values of pressure the flow is fully developed, since a non-zero slip velocity would depend only on the shear stress (first of Eqs. 19). The flow loses full development only after pressure decreases below a certain threshold that is determined through a parameter f that resembles the friction coefficient. Since such a threshold is reached for low

pressure values, this will likely occur close to the exit: here the slip velocity becomes pressure dependent and increases with decreasing pressure. Thus it seems reasonable that the experimental observations described in the previous sections would be reproduced.

The model proposed by Hill et al. (1990) and used also by Person and Denn (1997)

$$U_s = \alpha e^{-\beta p} {\tau_w}^m \ , \tag{20}$$

would give more difficulties in modeling the flow of the molten WPC of the present article: Eq. (20), in fact, basically predicts no slip at high pressure. As pressure decreases, the slip velocity does increase, but in a continuous and gradual way. As a result, it would not be possible to describe a flow that has both slip and full development at relatively high pressure values, such as the present one. The model proposed by the Kalyon and co-workers (see for instance Tang and Kalyon 2008), i.e.

$$U_s = \beta_0 \left(\frac{p_a}{p}\right)^{\kappa} {\tau_w}^m \left[0.5 + 0.5 \tanh\left(\alpha(\tau_w - \tau_c)\right)\right] \tag{21}$$

is similar to the model of Eq. (20), as reported by Tang (2012), thus it would behave similarly.

On the other hand, the model by Hatzikiriakos and Dealy (1992)

$$U_s = a(T)\left[1 - c\ \tanh\frac{E + b\frac{\sigma_w}{\tau_w}}{RT}\right] {\tau_w}^m \tag{22}$$

would most probably work: albeit, strictly speaking, the flow predicted using Eq. (22) is always non-fully developed, at high wall normal stress values (and constant temperature) the quantity in square brackets at the right hand side of Eq. (22) would tend to a constant, thus slip velocity would depend only on wall shear stress and would therefore be uniform for constant shear stress.

In this paper we have preferred to use Eq. (19) rather than Eq. (22) based on simplicity: the latter contains a total of seven material constants while the former only four parameters, namely λ, χ, m and f. Hatzikiriakos and Dealy's model is very complete since thermal and polymer microstructural features are taken into account, while they are not in in our model. However, it must be pointed out that Eq. (22) has been derived for the case of molten polymers, while the fluid that is presently studied is a suspension.

Now, collecting together the three equations (11), (16) and (19), we obtain the following system:

$$\begin{aligned} &\frac{dp}{dx} = -\frac{2}{H}\tau_w \\ &U_s = \begin{cases} \chi\,\tau_w^m & \tau_w \le fp \\ \chi\,\tau_w^m + \lambda\,(\tau_w - fp)^m & \tau_w > fp \end{cases} \\ &U = \begin{cases} U_s & \tau_w \le \tau_0 \\ U_s + \frac{n}{1+n}\frac{H}{2}\left(\frac{\tau_w}{k}\right)^{\frac{1}{n}}\left(1 - \frac{\tau_0}{\tau_w}\right)^{1+\frac{1}{n}}\left[1 - \frac{n}{1+2n}\left(1 - \frac{\tau_0}{\tau_w}\right)\right] & \tau_w > \tau_0 \end{cases} \end{aligned} \tag{23}$$

for the three unknowns p, U_s and τ_w . For any given value of U, it can be solved by specifying only one boundary condition, and this will be

$$p|_{x=L} = 0. \tag{24}$$

Eqs. (23) with the boundary condition (24) have been solved numerically. The solution scheme consists in discretizing the first equation of system (23) with the midpoint method to find pressure at the subsequent integration point. The second and third equations can then be used to calculate τ_w and U_s at the midpoints. In order to avoid numerical instabilities, it is more convenient not to use the boundary condition (24) directly, but to use a shooting method, guessing the pressure at the slit entrance

$$p|_{x=0} = P_0 \tag{25}$$

in such a way that pressure be 0 at the channel exit. A sufficiently accurate solution has been found with an axial length step of 10^{-1} mm over a slit length of 65 mm.

Once the axial velocity is known, the transverse velocity $v(x, y)$ can be obtained from the continuity equation:

$$\frac{\partial u}{\partial x} + \frac{\partial v}{\partial y} = 0 \tag{26}$$

by differentiating it once with respect to y

$$\frac{\partial^2 v}{\partial y^2} = -\frac{\partial^2 u}{\partial x \partial y} = -\frac{\partial \dot{\gamma}}{\partial x} \tag{27}$$

and integrating it twice subject to the following boundary conditions

$$v|_{y=0} = v|_{y=H/2} = 0 \qquad \forall\, 0 \le x \le L\,. \tag{28}$$

5. Model results and discussion

The material parameters that best fit the experimental pressure measurements are reported in Tab. 3. A good fitting has been obtained without using the yield stress as a parameter. This may indicate that even if the fluid had an yield point, this would be very small, possibly difficult to measure experimentally and of little significance for describing the flow under examination.

Tab. 3: Fitting parameters of the pressure dependent slip model described by Eqs. (12) and (19)

Herschel-Bulkley Eq. (12)			Slip law Eq. (19)			
$k\ \ (kPa\ s^{-n})$	n	$\tau_0\ \ (Pa)$	$\chi\ \ (m/s\ Pa^{-m})$	m	$\lambda\ \ (m/s\ Pa^{-m})$	f
23.4	0.407	0	$3.70\ 10^{-15}$	2.51	$5.54\ 10^{-15}$	0.0819

Tab. 3 also shows that the slip law exponent is almost equal to the reciprocal of the viscosity power law exponent, in agreement with De Gennes' theory (Brochard Wyart and De Gennes 1992) and also reported by Ebrahimi et al. (2015). Indeed, this would be almost true also with the two exponents of the model coming from the Mooney-Rabinowitsch procedure (see Tab. 1), but in the case of the exponents of Tab. 3 the agreement is much better.

In Fig. 8 the pressure vs. axial position plots are pictured for some representative cases and compared with the correspondent experimental pressure measurements. The model pressure profiles approximate the experimental data very well, denoting that the model captures the

essential physical phenomenon. Pressure falls linearly over the vast majority of the slit length and deviates from linearity only in the very last portion of the slit die, as expected.

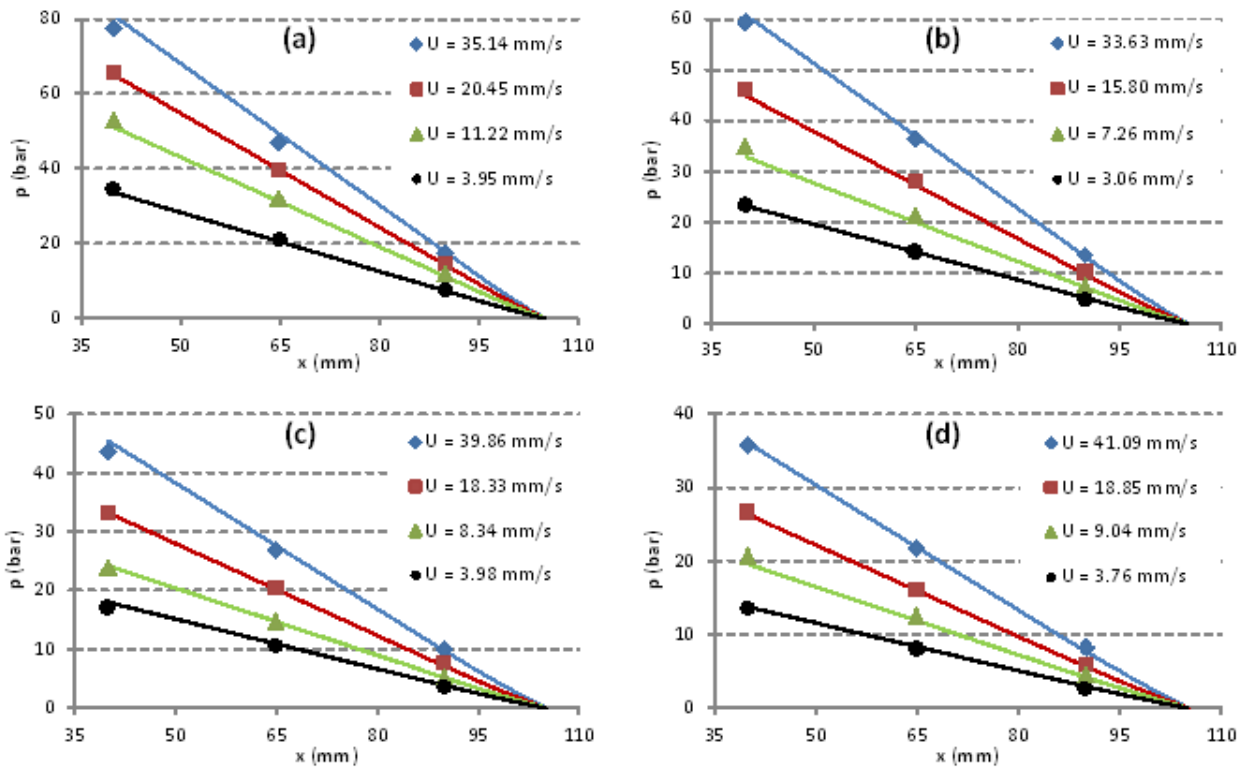

Fig. 8: Experimental pressure profiles compared with profiles coming from the pressure dependent slip model. The four plots are identified by the slit gap: (a) H = 1.95 mm, (b) H = 2.45 mm, (c) H = 3.31 mm, (d) H = 4.04 mm

The complete comparison between experimental and model data is reported in Tab. 4, which is analogous to Tab. 2. Again, experimental data are in white background, while the estimates using the model of the previous section are in green background. Tab. 4 reports also the absolute and relative errors with the same color notation as Tab. 2: red for overestimation, blue for underestimation. As can be seen, data fitting is globally more accurate than the model obtained from the Mooney-Rabinowitsch procedure (Tab. 2) and there is no qualitative error: overestimation and underestimation occur in fairly equal amount.

In Fig. 9 and 10 the slip velocity and wall shear stress profiles are shown for the same cases that are pictured in Fig 8. Slip velocity and wall shear stress are uniform in most of the channel, i.e. where the pressure profile is linear and the flow is fully developed. In the very last portion, where pressure loses linearity, slip velocity increases while wall shear stress decays. The behavior is basically identical to the one described by Hatzikiriakos and Dealy (1992) for their case of flow in long capillaries. From the quantitative point of view, the increase in slip velocity is quite remarkable, especially at high flow rates where slip may increase almost by 50%.

Tab. 4: Experimental pressure measurements compared with values coming from the pressure dependent slip model

		Experimental data			Pressure dependent slip			Absolute error			Normalized error		
H (mm)	U (mm/s)	p1 (bar)	p2 (bar)	p3 (bar)	p1 (bar)	p2 (bar)	p3 (bar)	p1 (bar)	p2 (bar)	p3 (bar)	p1 (%)	p2 (%)	p3 (%)
1.95	3.95	34.46	20.88	7.70	33.62	20.48	7.35	-0.85	-0.40	-0.36	-2.46	-1.92	-4.63
	6.20	42.32	25.44	9.01	40.27	24.54	8.80	-2.05	-0.91	-0.21	-4.84	-3.56	-2.28
	11.22	52.60	31.88	11.59	51.12	31.14	11.17	-1.48	-0.74	-0.42	-2.82	-2.32	-3.61
	13.83	57.48	34.56	12.42	55.59	33.87	12.14	-1.88	-0.70	-0.27	-3.28	-2.02	-2.19
	20.45	65.64	39.58	14.33	65.05	39.63	14.21	-0.59	0.05	-0.13	-0.90	0.13	-0.89
	29.97	73.64	44.50	16.32	75.83	46.20	16.56	2.19	1.70	0.24	2.98	3.82	1.45
	35.14	77.24	46.74	17.19	80.84	49.24	17.65	3.59	2.51	0.46	4.65	5.36	2.70
2.45	3.06	23.35	14.06	4.62	23.20	14.11	5.02	-0.15	0.05	0.41	-0.65	0.36	8.85
	7.26	34.67	21.07	7.38	32.82	19.96	7.10	-1.84	-1.10	-0.27	-5.32	-5.24	-3.68
	10.54	39.20	24.03	8.72	38.14	23.20	8.25	-1.06	-0.83	-0.46	-2.70	-3.46	-5.30
	13.30	42.19	25.64	9.12	41.88	25.47	9.06	-0.31	-0.17	-0.06	-0.72	-0.66	-0.62
	15.80	45.94	27.94	10.02	44.88	27.29	9.71	-1.06	-0.64	-0.31	-2.30	-2.30	-3.14
	22.57	51.30	31.38	11.54	51.79	31.50	11.20	0.49	0.12	-0.34	0.96	0.38	-2.95
	33.63	59.34	36.19	13.32	60.79	36.97	13.15	1.45	0.78	-0.17	2.44	2.16	-1.29
3.31	3.98	17.10	10.45	3.52	17.96	10.90	3.85	0.86	0.45	0.33	5.02	4.26	9.27
	8.34	23.83	14.61	5.15	24.18	14.67	5.18	0.35	0.07	0.02	1.48	0.46	0.48
	14.16	29.86	18.29	6.62	29.93	18.16	6.40	0.06	-0.14	-0.22	0.21	-0.76	-3.37
	18.30	33.00	20.31	7.49	33.18	20.13	7.10	0.18	-0.18	-0.39	0.55	-0.88	-5.21
	23.66	36.70	22.56	8.38	36.79	22.32	7.87	0.10	-0.24	-0.51	0.27	-1.07	-6.09
	29.65	38.39	23.46	8.40	40.29	24.44	8.61	1.90	0.98	0.22	4.95	4.18	2.60
	39.86	43.40	26.71	9.90	45.39	27.54	9.70	1.99	0.82	-0.20	4.58	3.09	-1.99
4.04	3.76	13.49	7.93	2.50	13.74	8.32	2.93	0.24	0.39	0.43	1.79	4.93	17.31
	6.06	17.06	10.16	3.46	16.65	10.08	3.55	-0.41	-0.08	0.09	-2.42	-0.78	2.54
	9.04	20.60	12.39	4.43	19.57	11.85	4.17	-1.04	-0.54	-0.26	-5.04	-4.35	-5.84
	18.85	26.56	16.07	5.91	26.30	15.93	5.60	-0.26	-0.14	-0.31	-0.98	-0.87	-5.17
	24.31	28.89	17.48	6.42	29.14	17.65	6.20	0.25	0.16	-0.21	0.88	0.94	-3.29
	31.76	31.82	19.31	7.12	32.45	19.65	6.91	0.63	0.34	-0.21	1.98	1.78	-2.95
	41.09	35.67	21.70	8.14	36.00	21.80	7.66	0.33	0.10	-0.48	0.94	0.45	-5.86

It is interesting to notice that the slit location where the flow loses full development is indeed quite close to the exit, but often well behind the position of the last pressure transducer. This means that the flow is really non-fully developed in spite of pressure measurements appearing linear, in agreement with the observations of Pieper et al. (2015) for the case of a non-colloidal suspension. As a consequence, it is not feasible from an experimental point of view to tell the beginning of non-full development from the non-linearity of the pressure profiles.

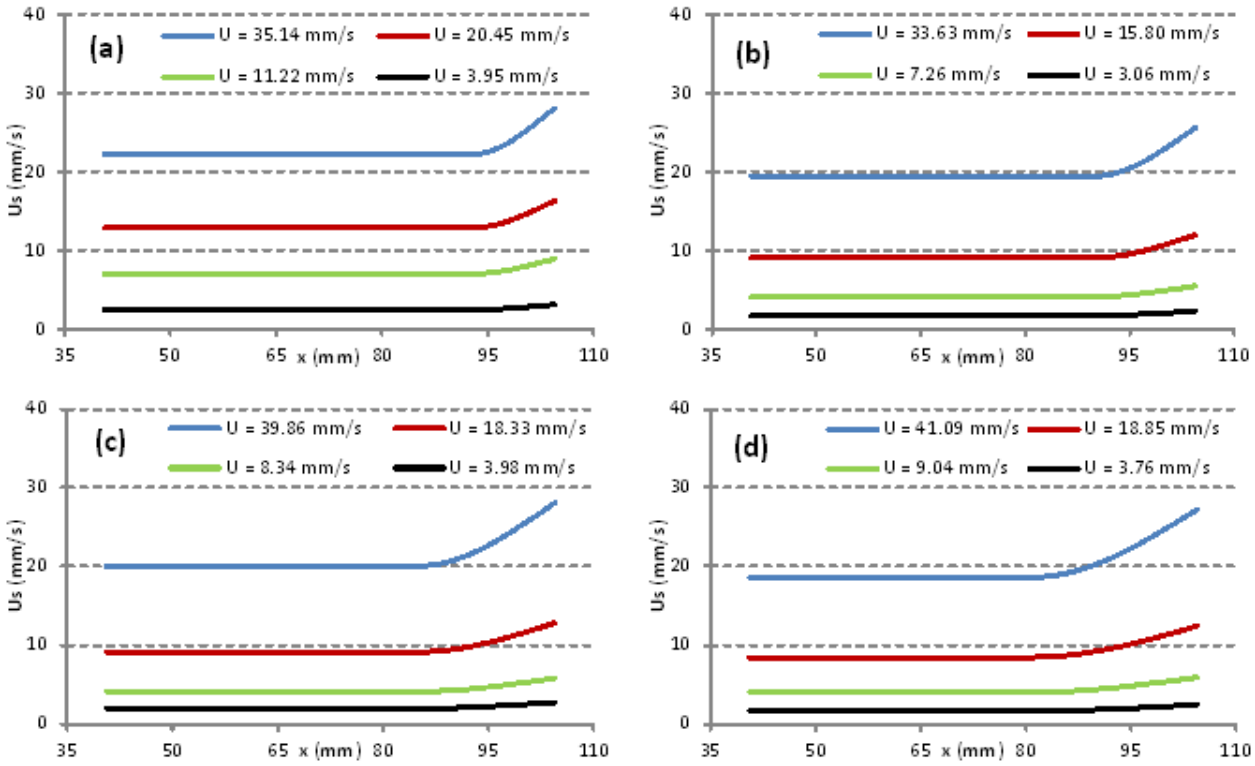

Fig. 9: Wall slip velocity profiles as predicted using the pressure dependent slip model. The four plots are identified by the slit gap: (a) H = 1.95 mm, (b) H = 2.45 mm, (c) H = 3.31 mm, (d) H = 4.04 mm

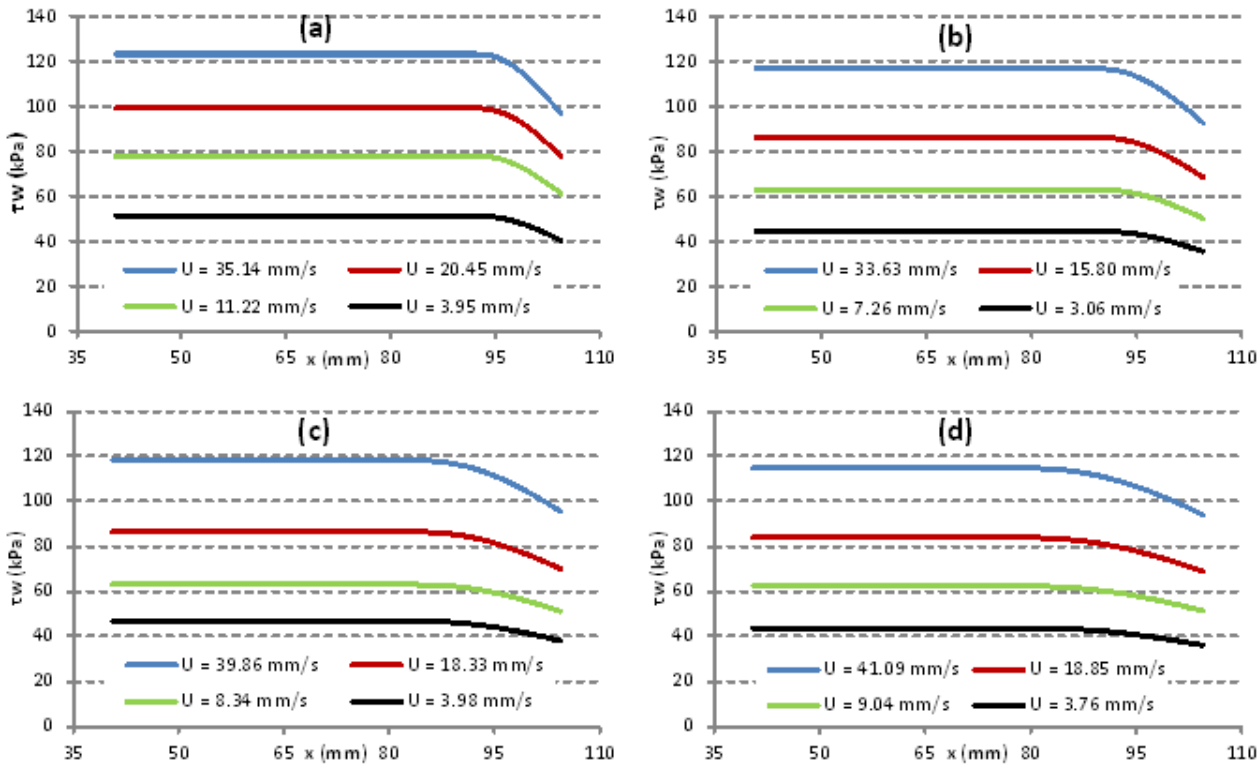

Fig. 10: Wall shear stress profiles as predicted using the pressure dependent slip model. The four plots are identified by the slit gap: (a) H = 1.95 mm, (b) H = 2.45 mm, (c) H = 3.31 mm, (d) H = 4.04 mm

Also, at equal shear stress the flow loses full development earlier for thicker slits. This is easy to explain by looking at Eq. (10): if wall shear stress and die length are constant, like in this case, pressure will be lower for wider gaps, thus the threshold for pressure dependent slip activation would be reached earlier.

However, this investigation has shown that pressure effects are important in a very short region close to the channel exit. This explains the reason why the viscosity parameters estimated through the Mooney-Rabinowitsch procedure are not too different from the ones obtained with the model introduced in the present article, as can be seen by comparing the corresponding data of Tab. 1 and Tab. 3. This is reasonable also because, in the determination of shear stress from experimental data, what matters is pressure gradient and not the absolute values of pressure: pressure can be measured modulo an additive constant without altering the shear stress evaluation. In the case of the slip law, on the other hand, the differences between the two models are more significant. It can be speculated that the slip velocities estimated on the basis of the Mooney-Rabinowitsch procedure are an average obtained by mediating over axial length. From Fig. 9 it can be seen that such an average value would be different from the slip velocity profile obtained by Eq. (19), especially at high flow rates and wide slit gaps.

From this point of view, notice from the Mooney plots of Fig. 3 that at each shear stress level the points that fall out of alignment mostly are indeed the ones for the smallest $1/H$ i.e. the points that are relative to the 4.04 mm slit gap. In particular, these points appear to lie slightly below a hypothetical line traced on the basis of the points relative to the other three gaps. This is due to the fact that at wider gaps the relatively lower pressure leads to a higher average slip velocity, which indeed corresponds to a steeper Mooney plot. This issue is explained in Fig. 11 and the main consequence is that usage of too wide slit gaps in the Mooney procedure is generally inappropriate for the materials studied in this paper.

The good fitting of the experimental data that has been obtained by the pressure dependent slip model may be viewed as a convincing argument about pressure dependent slip actually taking place. However, it must be pointed out that in the exit region of the slit die also temperature is lower (see Fig. 1), and this may somehow alter this result. On the other hand, experimental evidence shows that slip decreases with decreasing temperature (Hatzikiriakos and Dealy 1992) and moreover the local melt temperature reading could be greatly influenced by the surrounding steel die temperature. This is obviously lower due to the presence of the free surface at the exit, which is only 15 mm away. It is then possible that the fluid temperature is actually higher, possibly closer to the set temperature, in spite of the thermocouple reading. Thus, taking into account also that the temperature decrease that was measured is very small, of the order of 2.5 °C, it seems reasonable that the slip increase in the exit region be ascribed entirely to the pressure decrease.

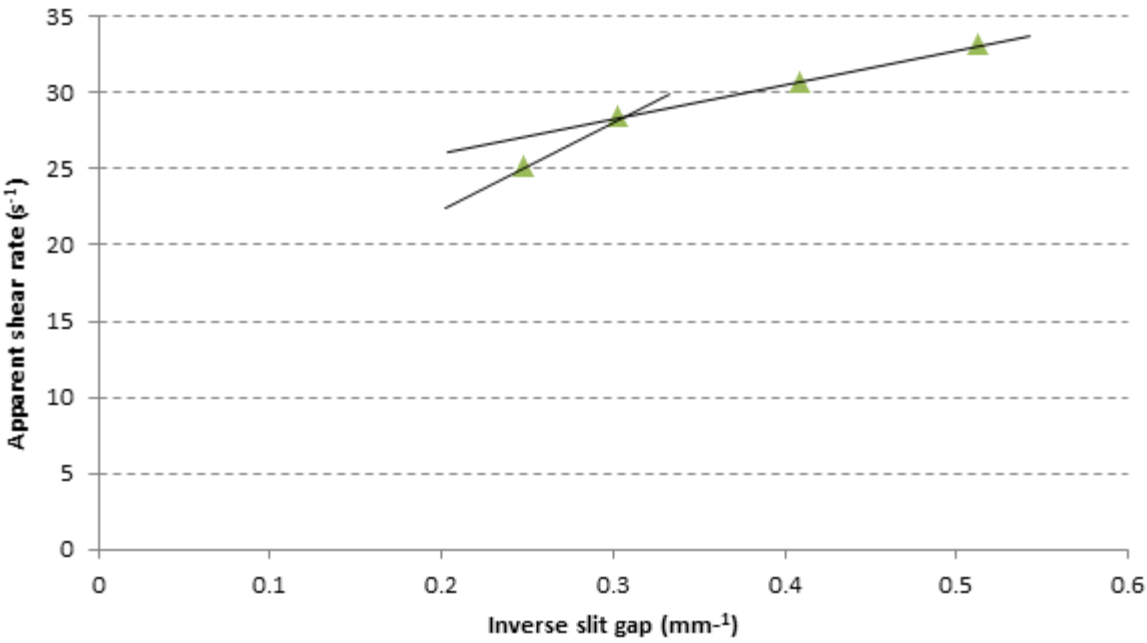

Fig. 11: Inaccuracy of the first point of the Mooney plot in the 80 kPa shear stress line. A Mooney line traced through the first two points is steeper than the one passing through the last three points.

Another possible source of inaccuracy of the results of this paper may originate from the different mixing conditions of the suspension traveling through the extruder. In fact, changing the die gap size has a direct effect on the counter-pressure inside the single screw extruder, which feeds the in-line rheometer. This in turn has an influence on the mixing capabilities of the extruder, in the sense that lower counter-pressure generally leads to less effective mixing. Mixing differences are known to generate variations in the rheological properties (see Kalyon et al. 2006b), therefore this is an important issue. On the other hand, in the present case the suspension is a commercial compound that has been pre-mixed by the compound supplier using a co-rotating twin screw extruder, therefore we are confident that mixing differences among the various flowing conditions, albeit present, might be negligible.

6. Conclusions

In this paper we have studied the rheological properties of a wood flour filled (50% wt.) polypropylene melt using a slit die rheometer attached to a single screw extruder. This instrument is particularly suited for this fluid because rheological characterization with the parallel plate rheometer in oscillatory mode may be ineffective due to difficulties in assuming the Cox-Merz rule to be valid for concentrated suspensions. Moreover, in the case of suspensions, there are problems related to the size of the suspended particles with respect to the rheometer gap size (Barnes 2000). Also capillary viscometry may not be a viable option due to the high viscosity induced by the large filler concentration and possible filtering effects (Yilmazer et al. 1989).

Four different slit gaps have been used in order to perform the Mooney procedure with sufficient confidence. Despite the Mooney procedure displays plots which are linear only in an approximate sense, a positive intercept with the apparent shear rate axis can be obtained, thus viscosity and wall slip velocity can be evaluated and modeled. On the other hand, if experimental pressure measurements are fitted with model predictions based on the previously evaluated viscosity and slip law, it can be seen that, despite being quite accurate from a quantitative point of view, the model data overestimate the experiments, especially at relatively low pressure values.

In order to explain this effect, another slip model possessing pressure dependence has been introduced. This has a total of seven parameters, i.e. three more than the one coming from the Mooney-Rabinowitsch procedure. One of the parameters, though, is the yield stress, which was eventually set to zero, making the number of additional parameters equal to two. Also, the exponent of the slip power law has been found to be basically equal to the reciprocal of the exponent of the Herschel-Bulkley constitutive equation for viscosity, in agreement with de Gennes' theory, thus reducing the number of parameters further.

The pressure dependent slip model approximates the experimental results better than the power law coming from the Mooney-Rabinowitsch procedure. On the other hand, since pressure effects can be seen only very close to the exit, the model from the Mooney-Rabinowitsch procedure and the one with pressure dependent wall slip do not differ too much, especially in the expression for viscosity.

The main result that has been obtained in the present work is that low pressure promotes wall slip of natural fiber filled polymeric fluids. This may have important implications for rheometry: strictly speaking the usual Mooney correction procedure is inapplicable, especially with relatively wide gaps, in which pressure effects are more relevant. Considering also that with wider gaps issues of secondary flows might become increasingly important, it is clear that the gap sizes which can be used for the Mooney procedure have an upper bound. Gap size is also bounded from below, since high suspension viscosity prevents from using gaps that are too narrow. In addition to this, a temperature increase, aiming at decreasing viscosity, is limited due to natural fiber thermal degradation. Putting everything together, it can be concluded that a precise rheological characterization of such fluids, in terms of viscosity and wall slip velocity, is a very challenging task. On the other hand, from the point of view of processing, pressure dependent slip plays a favorable role: the fluid motion tending to plug flow close to the die exit induces a smoother transition between the flow inside the slit and the motion of the solidifying extruded profile that leaves the extruder die, possibly leading to reduced flow exit instabilities.

References

Aral, B.K. and Kalyon, D.M. (1997). Viscoelastic material functions of noncolloidal suspensions with spherical particles. J. Rheol. 41 : 599 – 620

Barnes, H.A. (1995). A review of the slip (wall depletion) of polymer solutions, emulsions and particle suspensions in viscometers : its cause, character and cure. J. Non-Newtonian Fluid Mech. 56 : 221 – 256

Barnes, H.A. (2000). Measuring the viscosity of large-particle (and flocculated) suspensions – a note on the necessary gap size of rotational viscometers. J. Non-Newtonian Fluid Mech. 94 : 213 – 217

Brochard-Wyart, F. and de Gennes, P.G. (1992). Shear-dependent slippage at a polymer / solid interface. Langmuir 8 : 3033 – 3037

Damianou, Y., Georgiou, G.C., Moulitsas, I. (2013). Combined effects of compressibility and slip in flows of a Herschel-Bulkley fluid. J. Non-Newtonian Fluid Mech. 193 : 89 – 102

Ebrahimi M., Ansari, M., Hatzikiriakos, S.G. (2015). Wall slip of polydisperse linear polymers using double reptation. J. Rheol. 59 : 885 – 901

Gurunathan, T., Mohanty, S., Nayak, S.K. (2015). A review of the recent developments in biocomposites based on natural fibres and their application perspectives. Comp. Part A 77 : 1 – 25

Han, C.D. (1974). On slit and capillary die rheometry. J. Rheol. 18 : 163 – 190

Hatzikiriakos, S.G. and Dealy, J.M. (1992). Wall slip of molten high density polyethylenes. II. Capillary rheometer studies. J. Rheol. 36 : 703 – 741

Hill, D.A., Hasegawa, T., Denn, M.M. (1990). On the apparent relation between adhesive failure and melt fracture. J. Rheol. 34 : 891 – 918

Housiadas, K.D. (2013). Viscoelastic Poiseuille flows with total normal stress dependent, nonlinear Navier slip at the wall. Phys. Fluids 25 : 043105

Hristov, V., Vlachopoulos, J. (2007). A study of viscoelasticity and extrudate distortions of wood polymer composites. Rheol. Acta 46 : 773 – 783

Jastrzebski, Z.D. (1967). Entrance effects and wall effects in an extrusion rheometer during the flow of concentrated suspensions. Industrial & Engng. Chem. Fund. 6 : 445 – 454

Kalogirou, A., Poyiadji, S., Georgiou, G.C. (2011). Incompressible Poiseuille flows of Newtonian liquids with a pressure-dependent viscosity. J. Non-Newtonian Fluid Mech. 166 : 413 – 419

Kalyon, D.M. and Gokturk H.S. (1994). Adjustable gap rheometer. US Patent 5277058

Kalyon, D.M. (2005). Apparent slip and viscoplasticity of concentrated suspensions. J. Rheol 49 : 621 – 640

Kalyon, D.M., Gevgilili H., Kowalczyk, J.E., Prickett, S.E., Murphy, C.M. (2006a). Use of adjustable-gap on-line and off-line slit rheomters for the characterization of the wall slip and shear viscosity behavior of energetic formulations. J. Energetic Matls. 24 : 175 – 193

Kalyon, D.M., Dalwadi, D., Erol, M., Birinci, E., Tsenoglu, C. (2006b). Rheological behavior of concentrated suspensions as affected by the dynamics of the mixing process. Rheol. Acta 45 : 641 – 658

Li, T.Q. and Wolcott, M.P. (2005). Polym. Engng. Sci. 45 : 549 – 559

Mazzanti, V., Mollica, F. (2015). In-line rheometry of polypropylene based Wood Polymer Composites. Polym. Testing 47 : 30 – 35

Mazzanti, V., Mollica, F. (2016). Rheological and mechanical characterization of polypropylene-based wood plastic composites. Polym. Comp. 37 : 3460 – 3473

Mooney, M. (1931). Explicit formulas for slip and fluidity. J. Rheol. 2 : 210 – 222

Mourniac, P., Agassant, J.F., Vergnes, B. (1992). Determination of the wall slip velocity in the flow of a SBR compound. Rheol. Acta 31 : 565 – 574

Padmanabhan, M., Bhattacharya, M. (1994). In-line measurements of rheological properties of polymer melts. Rheol. Acta 33 : 71 – 87

Person, T.J. and Denn, M.M. (1997). The effect of die materials and pressure-dependent slip on the extrusion of linear low-density polyrthylene. J. Rheol. 41 : 249 – 265

Pickering, K.L., Efendy, M.G.A., Le, T.M. (2016). A review of recent developments in natural fibre composites and their mechanical performance. Comp. Part A 83 : 98 – 112

Pieper, S., Kirchhoff, N., Schmid, H. (2015). Absence of pressure sensitivity of apparent wall slip in pressure-driven flow of non-colloidal suspensions. Rheol Acta 54 : 69 – 75

Rao, I.J. and Rajagopal K.R. (1999). The effect of the slip boundary condition on the flow of fluids in a channel. Acta Mech. 135 : 113 – 126

Tang, H.S. and Kalyon, D.M. (2008). Unsteady circular tube flow of compressible polymeric liquids subject to pressure-dependent wall slip. J. Rheol. 52 : 507 – 525

Tang, H.S. (2012). Analysis on creeping channel flows of compressible fluids subject to wall slip. Rheol. Acta 51 : 421 – 439

Vinogradov, G.V. and Ivanova, L.I. (1967). Viscous properties of polymer melts and elastomers exemplified by ethylene-propylene copolymer. Rheol. Acta 6 : 209 – 222

Walters, K. (1975). Rheometry, Wiley, New York

Yilmazer, U., Gogos, C.G., Kalyon, D.M. (1989). Mat formation and unstable flows of highly filled suspensions in capillaries and continuous processors. Polym. Comp. 10 : 242 – 248